ORIGINAL RESEARCH ARTICLE

# Determination and Modeling of the Plastic-Flow Behavior of a Strain- and Strain-Rate-Hardening Material *via* the Constant-Stress, Constant-Heating-Rate Test

S.L. SEMIATIN, N.C. LEVKULICH, P.N. FAGIN, T.M. BUTLER, T.J. BENNETT IV, and E.M. TALEFF

The high-temperature plastic-flow behavior of a strain- and strain-rate-hardening material was quantified using a novel, high-throughput technique known as the constant-stress, constant-heating-rate (CSCHR) test. For this purpose, CSCHR experiments were performed on annealed sheet of unalloyed (Type 1) niobium using three constant-stress levels (34, 69, and 103 MPa) and two heating rates (15 and 63 °C/min). To interpret the observations, a suite of relations was derived to enable the extraction of the material coefficients that describe the constitutive behavior (*i.e.*, apparent activation energy $Q$, strain hardening exponent $p$, strain-rate sensitivity exponent $m$) from the CSCHR measurements. Among other things, the relations revealed that the value of $Q$ is a function of the slope of the Arrhenius plot as well as a term dependent on the ratio of $p$ to $m$. It was also demonstrated that the same material coefficients describing behavior during the continuous heating imposed during CSCHR tests were applicable for quantifying deformation under isothermal, constant-strain-rate conditions within a reasonable engineering accuracy.

https://doi.org/10.1007/s11661-024-07614-2


## I. INTRODUCTION

BODY-CENTERED-CUBIC refractory metals and alloys have long held promise for applications involving service temperatures comparable to and much higher than those that can be accommodated by titanium alloys, nickel- and cobalt-base superalloys, *etc.*, *i.e.*, $T > 1100$ °C.[1–4] Much of this benefit results from the higher melting points of such materials and excellent mechanical properties that can be achieved by solid-solution and precipitation hardening. Despite such attributes, however, a number of challenges limiting their widespread utilization still remain. These include difficulties associated with thermomechanical processing, low (or nil) ambient-temperature ductility, and limited oxidation resistance, let alone the limited number of facilities available for the high-temperature characterization of such materials.[5–8] Approaches to remedy these problems have been based on alloying-element additions (*e.g.*, addition of rhenium to tungsten), the generation of an ultrafine or deformed microstructure, and the development of new classes of alloys such as refractory high-entropy alloys (RHEAs) and refractory complex-concentrated alloys (RCCAs).[9,10]

In some respects, the difficulty of high-temperature testing to quantify the mechanical properties of refractory metals and alloys including the determination of the effect of various alloying elements on behavior has also served as a roadblock to the development of design allowables for existing and emerging materials in this class. Often, such tests must be conducted at temperatures in the range of 1000 °C to 1800 °C under vacuum (or inert) conditions to avoid test-coupon contamination. Obtaining a large quantity of data can thus be very time consuming and expensive. The development of methods for the rapid determination of high-temperature properties such as creep resistance, ductility, *etc.* would therefore be very helpful in the design-and-selection process for refractory metals.

Recently, a high-throughput method to characterize the plastic-flow behavior of ductile metals has been developed.[11] The approach comprises the application

S.L. SEMIATIN, N.C. LEVKULICH, and P.N. FAGIN are with the Air Force Research Laboratory, Materials and Manufacturing Directorate, Wright-Patterson Air Force Base, OH 45433-7817 and also with MRL Materials Resources LLC, Xenia Township, OH 45385. Contact e-mail: slsemiatin@icmrl.net T.M. BUTLER is with the Air Force Research Laboratory, Materials and Manufacturing Directorate. T.J. BENNETT IV and E.M. TALEFF are with the Department of Mechanical Engineering, The University of Texas, Austin, TX 78712.
Manuscript submitted April 3, 2024; accepted September 27, 2024.
Article published online October 21, 2024

of a constant true stress during sample heating at a constant rate while measuring the plastic deformation as a function of time. The utility of such constant-stress, constant-heating-rate (CSCHR) tests was demonstrated initially using a tensile mode of loading for sheet product of unalloyed titanium, an $\alpha/\beta$ titanium alloy, and superalloy 718. Due to the development of diffuse necking during tension testing of ductile metals, flow-localization analyses for the CSCHR test have also been performed to aid in the reduction of strain-*vs*-temperature data.[12] The resulting Arrhenius plots enable the determination of constitutive parameters (such as the apparent activation energy $Q$ and stress exponent of the strain rate $n$), the effect of texture on plastic flow, *etc*.[11,12]

Prior work on the CSCHR test focused largely on deformation at high temperatures in what is nominally considered to be the hot-working regime. Under such conditions, metallic materials typically exhibit little to no strain hardening except at relatively low strains ($\leq 0.1$). In such cases, a constitutive description based largely on the values of $Q$ and $n$ and a temperature-compensated strain rate (Zener-Hollomon parameter) is usually sufficient to describe creep-like behavior. By contrast, at lower temperatures, *i.e*., in the warm-deformation regime, the plastic flow of metallic materials normally exhibits both substantial strain hardening *and* strain-rate hardening. It might be expected that the description of plastic flow in this domain would be somewhat more complex than that in the hot-working domain. To circumvent such challenges, attention is often restricted to relatively low or high strains, and simplified constitutive models analogous to those at hot-working temperatures are fitted to experimental measurements.

The objective of the present work was to establish the suitability of the CSCHR test method to quantify constitutive response over a wide temperature range *under deformation conditions involving both strain hardening and strain-rate hardening*. For this purpose, unalloyed (reactor grade) niobium (Type 1[13]) was chosen as a model material based on its high melting point (2468 °C) and, hence, broad warm-working range. In addition, its deformation under isothermal (and non-isothermal) conditions has been thoroughly baselined in the literature *via* constant-stress compression creep,[14] "temperature-shift" tensile creep,[15] constant-true-strain-rate compression,[16] and constant-true-strain-rate tension.[17,18] These prior efforts have been well summarized by Brady and Taleff.[17,18] With respect to constitutive response, their summary revealed a noticeable temperature dependence (*unfortunately with substantial scatter*) in measurements of the apparent activation energy for temperatures between 800 °C and 1900 °C. Less information regarding strain and strain-rate hardening are available, however, aside from their own *isothermal* data, thus providing additional impetus for undertaking the present research.

## II. MATERIALS AND PROCEDURES

### A. *Materials*

Type 1 niobium (hereafter referred to simply as niobium) was used to establish a CSCHR-based methodology for determining the material coefficients for constitutive relations pertinent to plastic flow in the warm-deformation regime. The research material came from the same lot as that used in Reference 17. In particular, it was received as 0.51-mm-thick sheet with measured impurity levels (in wppm) of 9 C, 60 N, 73 O, 3 H, 5 Zr, 300 Ta, 5 Fe, 10 Si, 33 W, < 5 Ni, < 10 Mo, 10 Hf, and < 5 Ti. CSCHR test samples were electrical-discharge machined (EDM'ed) with the tension axis (TA) parallel to the original rolling direction (RD) of the sheet. Each sample had a geometry similar to that reported previously.[11] It comprised a dog-bone shape with a gage section measuring 3.2 mm wide × 19.1 mm long. To remove any residual dislocation substructure in the as-received alloy, the material was annealed at 1200 °C for 1 hour. For this purpose, each individual test sample was encapsulated in a quartz tube (which was evacuated and backfilled with high-purity (0.99999) argon) prior to heat treatment in an electric-resistance furnace. Following annealing, each capsule was air cooled.

### B. *Experimental Procedures*

Per the detailed description in Reference 11, CSCHR tests were performed in a vacuum chamber (evacuated to ~ $10^{-6}$ torr) located within a screw-driven, computer-controlled Instron machine. Following pump-down, each sample (containing a thermocouple spot welded at the mid-length of the reduced section) was heated (under a very small load of ~ 10 N to prevent buckling) to and soaked at 704 °C for 10 minutes; following the soak period, an axial load corresponding to a true stress of either 34, 69, or 103 MPa was applied. Samples were then heated (and deformed under constant-true-stress (load-controlled) conditions) at a constant rate of 63 °C/min until failure (as occurred in all tests except one) or a peak temperature of 1510 °C was reached. Additional samples were tested using stress levels of 34 or 103 MPa and a heating rate of 15 °C/min. At the end of testing, power to the heating elements was turned off, and the sample and tooling were cooled.

The principal data from each CSCHR test consisted of a plot of the plastic strain as a function of time/temperature, from which an Arrhenius plot (ln strain rate-*vs*-inverse absolute temperature) was derived. Each Arrhenius plot (and the corresponding best-fit slope determined *via* linear-regression analysis) was generated from *unsmoothed* strain (and, thus, strain rate) data as a function of inverse absolute temperature. A complementary second approach utilized strain-*vs*-time/temperature data that were first *smoothed* using a digital

second-order Butterworth lowpass filter applied in both the forward and backward directions to eliminate phase shift.[19,20] The filter cutoff frequency was 0.1 Hz, and the sampling frequency was 5 Hz. Filtering artifacts at the start and end of the strain-*vs*-time data were suppressed by padding the measurements using the following parameters: padding length = 50 and padding type = odd. The strain rates were then calculated from the smoothed strain (and time) data using a second-order central-difference method implemented in Python. For both methods, data cutoff was imposed for very low strain rates (below ~ $10^{-4}$ $s^{-1}$) at which strain resolution was poor and at high strains and strain rates at which non-uniform plastic flow had occurred. The latter limit was evidenced by noticeable upturns in the Arrhenius plots, a behavior previously analyzed using classical flow-localization simulations (Appendix in Reference 12).

To determine whether the material parameters determined from CSCHR tests could also be used to describe the constitutive behavior deduced from conventional mechanical tests, several isothermal tension tests were also performed on the annealed samples. These latter experiments were conducted in the same screw-driven system as the CSCHR tests. They involved preheating to a temperature of 1200 °C or 1330 °C, soaking for 10 minutes to minimize grain growth, and pulling at a constant true strain rate of 0.001 $s^{-1}$. The measured load–stroke curves were converted to true stress–true strain assuming uniform deformation restricted to the reduced section. The applicability of this assumption as well as the reliability of the values of the constitutive parameters were established by flow-localization simulations of the isothermal tension test using the load-equilibrium method.[21]

As-received, as-annealed, and annealed samples that had been subjected to CSCHR tests were characterized using electron backscatter diffraction (EBSD) in a ThermoFisher Apreo C scanning electron microscope (operated at 20 kV, a spot size of 17, and working distance of 25 mm) that was outfitted with an Oxford Symmetry EBSD detector. For this purpose, analysis was done on rolling-direction (RD) cross sections (containing the rolling and sheet-normal (SN) directions), for the starting materials, and on in-plane sections (containing the RD and long transverse (TD) directions) for deformed samples. Both types of sections were prepared using standard metallographic techniques. For the in-plane samples, the entire thickness of the sheet was mounted and then ground and polished to the midplane.

Using a step size of 0.4 $\mu$m, EBSD data were collected over an area measuring 200 × 250 $\mu$m for the starting (undeformed) microstructures. The microstructure and texture of deformed samples were determined by EBSD of the entire reduced section, the fillet region, and a portion of the shoulder. In these cases, the step size was 5 $\mu$m. Small patches of each sample (measuring ~ 0.5 × 2 mm) were also inspected using a step size of 0.5 $\mu$m.

To assess the possible need to consider texture hardening or softening on observed flow hardening and, thus, to isolate true strain-hardening behavior, Taylor factors for the undeformed (annealed) material in the shoulder and the deformed material in the gage section of tested samples were estimated with the EDAX EBSD software package. Inputs to the calculations consisted of (i) the EBSD-measured textures, (ii) values of the strain-increment ratio during tension testing, and (iii) the critical resolved shear stresses (CRSS's) for the pertinent slip systems. Two different sets of strain-increment ratios were used in the calculations, one characterized by a normal plastic anisotropy ratio ($r$ value) of unity ($r = d\varepsilon_w/d\varepsilon_t$, in which $\varepsilon_w$ and $\varepsilon_t$ denote the instantaneous values of the width and thickness strains, respectively, during deformation) and the other by $r = 3$. The value of $r = 3$ was estimated based on the measured width and thickness strains at each of two axial locations in fractured CSCHR samples. Deformation was assumed to have occurred by slip along <111> directions on {110}, {112}, and {123} planes (*i.e.*, an approximation of pencil glide) with the CRSS assumed to be equal for all three slip modes.

## III. RESULTS

The key results of this work consisted of characterization of the starting (as-received *vs* annealed) microstructures and textures, CSCHR and isothermal tension-test measurements, and the deformed textures/$r$ values for selected deformed samples.

### A. *Starting Microstructures and Textures*

Determined using EBSD, inverse-pole-figure (IPF) maps (for the original rolling direction of the sheet), inverse pole figures, and kernel-average-misorientation (KAM) maps quantified the starting microstructure, texture, and level of stored work, of the unalloyed niobium (Figures 1 and 2) in both the as-received condition and the annealed condition (on which mechanical testing was done). Material in the as-received condition [Figures 1(a) and 2(a)] exhibited a slightly distorted grain structure (average circle-equivalent diameter, or CED, of ~ 12 $\mu$m), a moderate-strength (4.5 × random) texture with a principal component consisting of <111> poles lying parallel to the SN direction of the sheet, and moderate levels of stored work (maximum KAM ~ 1.5 deg).

Characterization of the sheet given a 1-hour anneal at 1200 °C [Figures 1(b) and 2(b)] revealed a fully recrystallized grain structure (average CED of ~ 41 $\mu$m) with essentially no residual lattice curvature and a moderate-strength (4 × random) texture consisting of <101> and <112> poles parallel to the original RD. In comparison to the as-received material, the increase in grain size by a factor of ~ 3.5 also suggested a fully-annealed structure.

A grain size of 40 $\mu$m would result in ~ 1000 grains in a section across the gage width, thus ensuring good

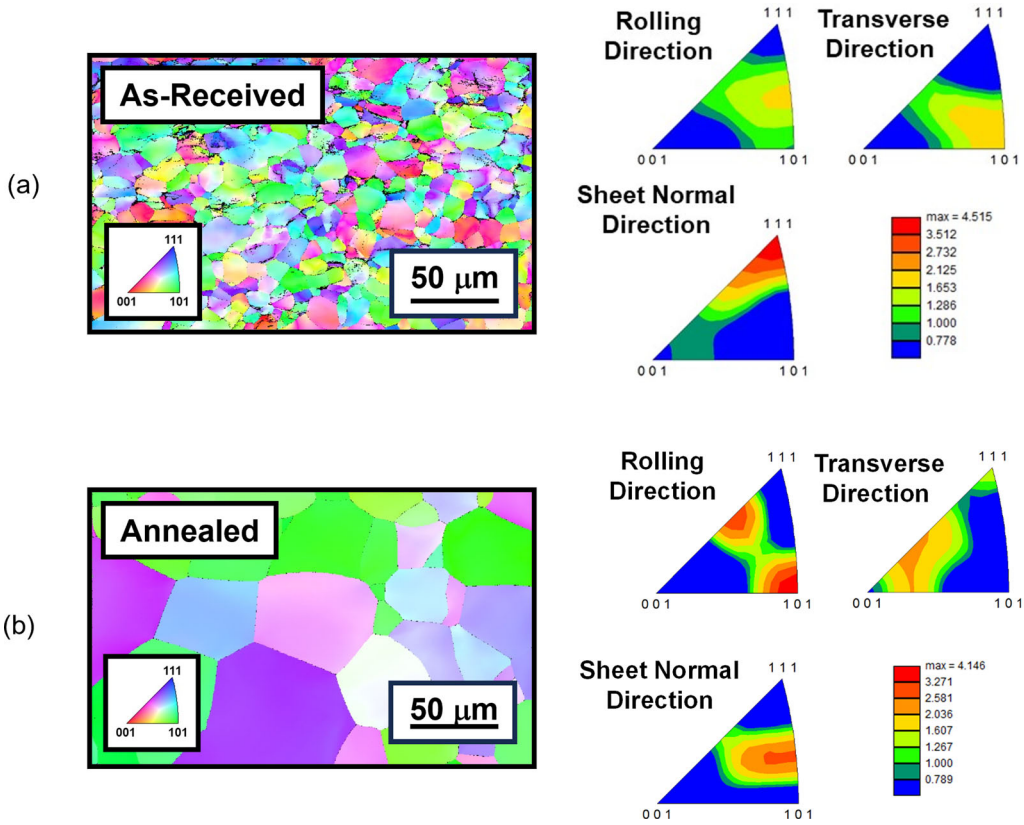


Fig. 1—EBSD data comprising RD IPF maps and inverse pole figures for the niobium sheet material: (*a*) As-received and (*b*) annealed 1200 °C/1 h (Color figure online).

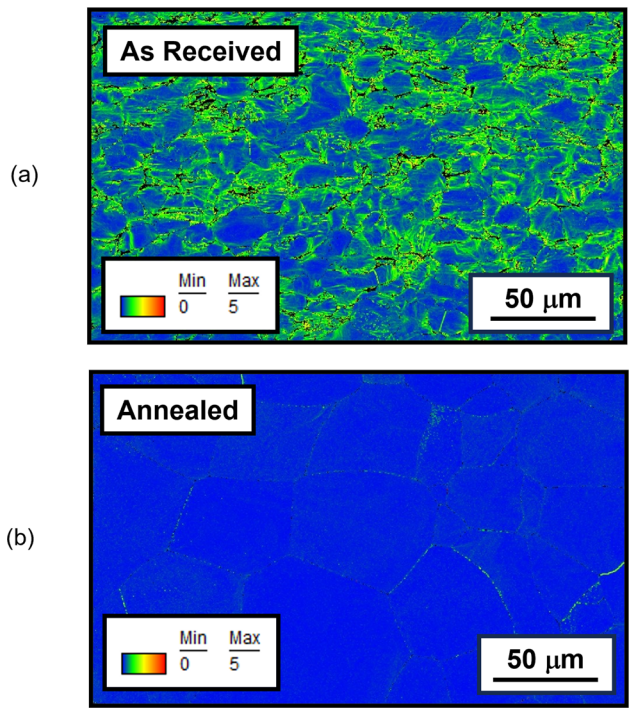


Fig. 2—EBSD-determined KAM values (in degrees) for the niobium sheet material: (*a*) As-received and (*b*) annealed 1200 °C/1 h (Color figure online).

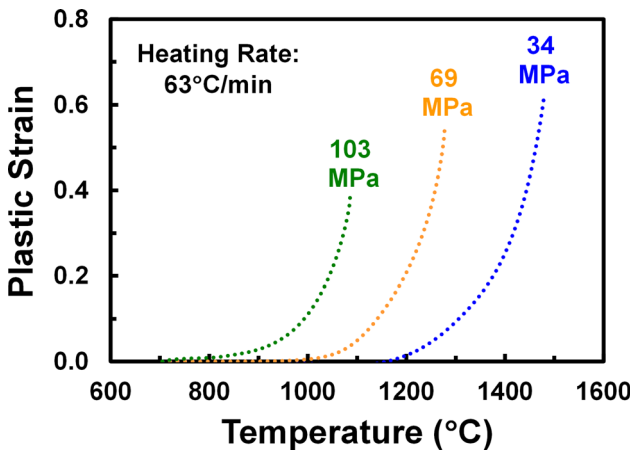


Fig. 3—Plastic strain as a function of temperature from constant-stress ($\sigma$ = 34, 69, 103 MPa), constant-heating-rate (63 °C/min) experiments on annealed niobium sheet tested along the original RD of the sheet.

sampling statistics for the sample geometry chosen for the experimental work.

## B. *CSCHR Data*

For each level of the applied stress and heating rate, measurements of the plastic strain as a function of temperature from CSCHR tests (*e.g.*, Figure 3 for

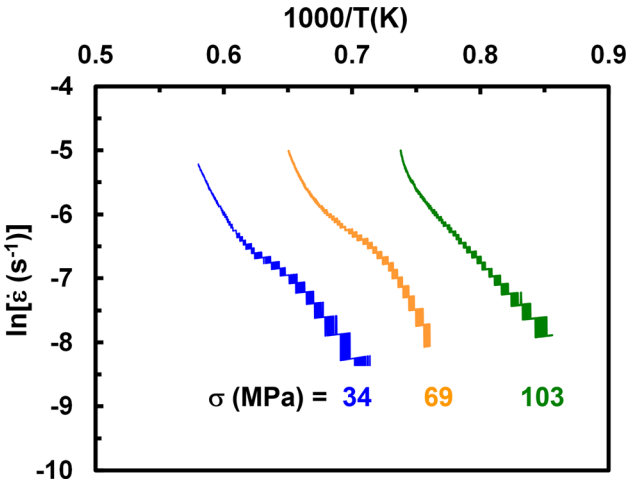


Fig. 4—Arrhenius plots of $\ln\dot{\varepsilon}$ *vs* 1000/*T*(K) derived from the CSCHR data in Fig. 3 for annealed niobium sheet material tested using a stress of 34, 69, or 103 MPa and a heating rate of 63 °C/min.

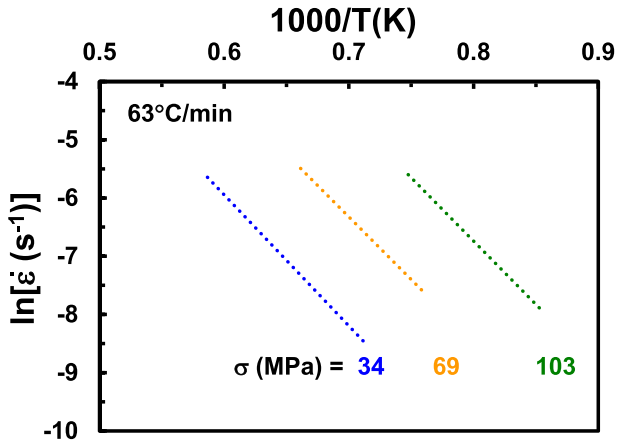


Fig. 5—Arrhenius plots derived from the smoothed strain-*vs*-temperature/time CSCHR data in Fig. 3 for annealed niobium sheet material. The "noisy" low-strain-rate data and flow-localization-affected high-strain-rate data were truncated before determining the best-fit, linear-regression slope for each plot.

heating rate = 63 °C/min) showed a similar shape. As found for previous CSCHR data for titanium- and nickel-based alloys in the hot-deformation regime,[11,12] the shapes of all the deformation transients (Figure 3) indicated an increase in the rate of straining with increasing temperature. Furthermore, the onset of rapid straining was delayed to higher temperatures when using lower applied stresses.

Using *unsmoothed* strain-*vs*-temperature/time data, the corresponding Arrhenius plots in terms of the natural logarithm of the plastic strain rate ($\dot{\varepsilon}$) as a function of inverse absolute temperature ($1/T$(K)) each showed a nearly linear trend (Figure 4) except at low and high values of $\ln\dot{\varepsilon}$. As mentioned in Section II–B, "noise" in the plots for *low values* of $\ln\dot{\varepsilon}$ resulted from the difficulty of taking the derivative of strain-*vs*-time data for low values of strain/strain rate. For the *high-strain-rate* regime, the "upturn" in each Arrhenius plot in Figure 4 indicated the onset of flow localization in tension.[12] Disregarding such regions and using the smoothed strain-*vs*-temperature/time data led to the results displayed in Figure 5 for a heating rate of 63 °C/min. The slopes of the fitted straight lines (Table I) and the strain rate–temperature data *per se* (Figure 5) revealed a noticeable similarity at the various levels of applied stress.

The effect of heating rate on CSCHR behavior was elucidated by comparing data obtained using samples heated at either 15 °C/min or 63 °C/min and a stress of 34 or 103 MPa (Figure 6). For a given stress, the 15 °C/min curve was shifted to lower temperatures compared to that observed for a heating rate of 63 °C/min. Such behavior can be rationalized based on the longer times available for straining at a given temperature at the lower heating rate. Despite this shift, the Arrhenius plots for the 15 °C/min tests (not shown) still exhibited a slope (23,000 K) almost identical (within experimental scatter) to those measured for the same material tested at the higher heating rate, *i.e.*, ~ – 22,000 K, as summarized in Table I. Because of the strain-hardening nature of Type 1 niobium (and other metals) in the warm-working regime, however, the Arrhenius slopes do *not* correspond to a gas-constant-normalized value of apparent activation energy, $Q/R$. The interrelation between such quantities is interpreted in detail in Section IV.

### C. *CSCHR Microstructure and Texture Evolution*

EBSD inverse-pole-figure (IPF) maps for the tension axis, KAM maps, and inverse pole figures for annealed niobium samples taken to failure provided insight into microstructure evolution and texture formation in the niobium material subjected to CSCHR testing. In particular, IPF maps for samples heated at a rate of 63 °C/min and deformed using a stress of 34 or 103 MPa exhibited extremes in behavior (Figure 7).

For the sample deformed using $\sigma$ = 34 MPa, which failed at ~ 1485 °C (Figure 3), the IPF and KAM maps [Figures 7(a), (b)] exhibited large equiaxed grains and almost no residual misorientation, respectively. These features were strongly suggestive of *static* recovery or recrystallization after testing, which can be attributed to moderately slow cooling (~ 60 °C/min) in the vacuum furnace following testing. The absence of *dynamic* recrystallization at such temperatures was also evident in the *flow-hardening* response observed during isothermal high-temperature tests performed in the present work (to be discussed in the next section) as well as those conducted by Brady and Taleff.[17]

The sample deformed using $\sigma$ = 103 MPa failed at ~ 1100 °C, a temperature below that at which static recrystallization occurs. The IPF map for this sample [Figure 7(c)] exhibited elongated grains, many with noticeable gradations in color indicating substantial lattice curvature and, thus, retained work. The preponderance of green color in the IPF map also suggested that the deformed texture was dominated by <101> poles close to the tension axis. The associated KAM map for this sample [Figure 7(d)], dominated by yellow

and red colors, also indicated substantial lattice misorientation, *i.e.*, in the range of 2.5 to 5 deg. These values were much greater than the KAM level for the as-received material [Figures 2(a)] as well as the fully-annealed condition of course [Figure 2(b)].

Inverse pole figures for the tension axis (which was parallel to the original rolling direction of the sheet) of the sample that was deformed using $\sigma = 103$ MPa and a heating rate of 63 °C/min (Figure 8) further illustrated how texture evolved. The figure compares the starting (annealed) texture [Figure 8(a)] to the average texture of the entire gage section after failure [Figure 8(b)], and a 2.5-mm-long region adjacent to the fracture site [Figure 8(c)]. The results indicated the loss of the <112> and the strengthening of the <101> poles due to deformation. Likely due the development of a diffuse neck prior to fracture, the strengthening of the <101> poles was most prominent for the region lying closest to the fracture [Figure 8(c)]. Such rotations were expected based on the present starting (annealed) texture and the rotations predicted for bcc crystals deforming by pencil glide.[22] (It should be noted that the calculations in Reference 22 were for axisymmetric *compression*, for which poles rotate in directions opposite to those for axisymmetric *tension*.)

Calculated average Taylor factors ($M$) for *unrecrystallized* samples revealed a relatively small degree of texture hardening during the CSCHR tests (Table II). Assuming $r = 3$ (per measurements of width and thickness strains on broken samples), the Taylor factor increased slightly from ~ 3.04 (measured in the undeformed shoulders of samples) to ~ 3.13 (in high strain regions near the fracture sites). Corresponding changes in Taylor factor for the hypothetical case of $r = 1$ were from ~ 2.93 to ~ 2.98.

The limited amount of texture hardening in the present work (*i.e.*, ~ 2 to 3 pct. based on the peak strains near the fracture sites, and more likely magnitudes of one-half these values if based on average strains in the reduced section) can also be rationalized in terms of Taylor-factor calculations in the Rosenberg and Piehler work[22] for an imposed *axisymmetric* compression (or tension) state of strain. For texture components near <101> and <112>, the predicted Taylor factors were ~ 3.0 and ~ 2.8, respectively. The maximum Taylor factor of 3.18 was calculated for a sharp texture located exactly at the <101> pole. The crystal rotations noted in the present work, which gave rise to the measured, slight texture hardening from $M \sim 3$ to $M \sim 3.1$ were thus concluded to be as expected from the prior aggregate-theory calculations. The moderately high r values measured on broken tension samples (*i.e.*, $r \sim 3$) were also as expected based on the starting IPFs for this condition [Figure 1(b)]. Specifically, a comparison with the Rosenberg and Piehler results[22] revealed that the transverse (width) and sheet normal directions of the annealed samples corresponded to relatively soft and relatively hard initial orientations, respectively, which in turn would produce $r$ values noticeably greater than unity, as was observed.

### D. *Isothermal Tension Test Data*

Flow curves from the selected isothermal tension tests conducted at a constant true strain rate of 0.001 $s^{-1}$ revealed a yield stress followed by flow hardening to a true strain between approximately 0.4 and 0.5 [Figure 9(a)]. Due to the limited change in texture during tension testing, as discussed in Section III–C, the measured flow hardening can be ascribed to strain hardening *per se*. The apparent softening at high strains was due to flow localization in a diffuse neck that led to through-thickness necking along a zero-extension direction (at ~ 55 deg to the tension axis) and final fracture. Thus, the assumption of uniform deformation used to reduce the load-stroke results did not apply for strains in excess of ~ 0.4. Such an interpretation was validated by flow-localization calculations to be presented in Section IV.

When the true stress–true strain data for strains less than or equal to ~ 0.35 were replotted in ln–ln terms [Figure 9(b)], the nearly linear slopes suggested that strain hardening could be described by a simple power law with a strain-hardening exponent of 0.17. For the experiment performed at 1330 °C, a deviation from linearity was noted at $\ln\varepsilon \approx -4.5$ (corresponding to $\varepsilon \sim 0.01$) and lower; this may be ascribed to experimental uncertainty.

## IV. DISCUSSION

The present work has shown that the plastic flow in the warm-deformation regime during CSCHR and (selected) isothermal tension tests for unalloyed (annealed) niobium is a function of applied stress, heating rate, and strain (and strain-rate) hardening. In this section, a unified approach is presented, which can model both types of measurements. The analysis was based on the use of a simple phenomenological constitutive equation whose material constants are readily ascertained.

In the sections below, the equations needed to extract material coefficients from CSCHR data are presented first, the coefficients are shown to be capable of modeling the observed plastic-flow observations for the entire range of CSCHR measurements for niobium, and an analysis of the isothermal tension–test observations is used to demonstrate the consistency of the approach for both types of deformation mode.

### A. *Constitutive Model and Determination of Material Coefficients*

In the past, analyses of *isothermal* deformation focused primarily on constitutive models which describe the inter-dependence of stress, strain rate, and temperature for applications such as creep, superplasticity, and conventional bulk forming *in the hot-deformation regime*. Typically, the approaches utilized the concept of the temperature-compensated strain rate ($Z =$

Table I. Slopes ($10^3$ K) of $\ln\dot{\varepsilon}$ *vs* $1/T$(K) (Arrhenius) Plots for Annealed Nb

| Heating Rate (°C/min) | $\sigma$ = 34 MPa | $\sigma$ = 69 MPa | $\sigma$ = 103 MPa |
|---|---|---|---|
| 63 | − 22.5/− 21.9 | − 21.5/− 22.5 | − 21.7/− 22.3 |
| 15 | − 23.2/— | — | − 23.0/— |

The first number of each pair was derived using unsmoothed data, and second using smoothed data.

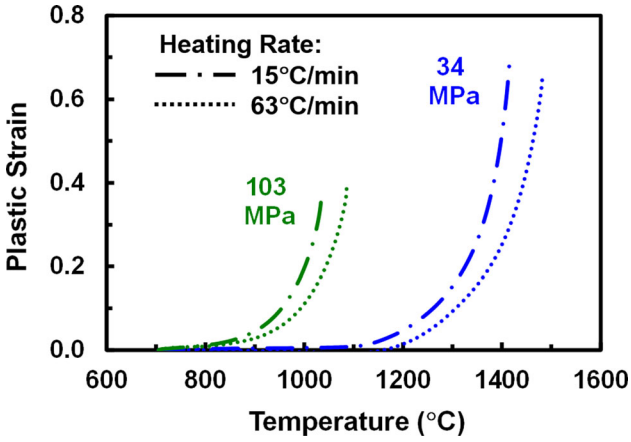


Fig. 6—Comparison of plastic strain as a function of temperature measurements from CSCHR tests using a constant stress ($\sigma$ = 34 MPa or 103 MPa) and two different constant heating rates (15 °C/min, 63 °C/min) for annealed niobium samples tested along the original RD of the sheet.

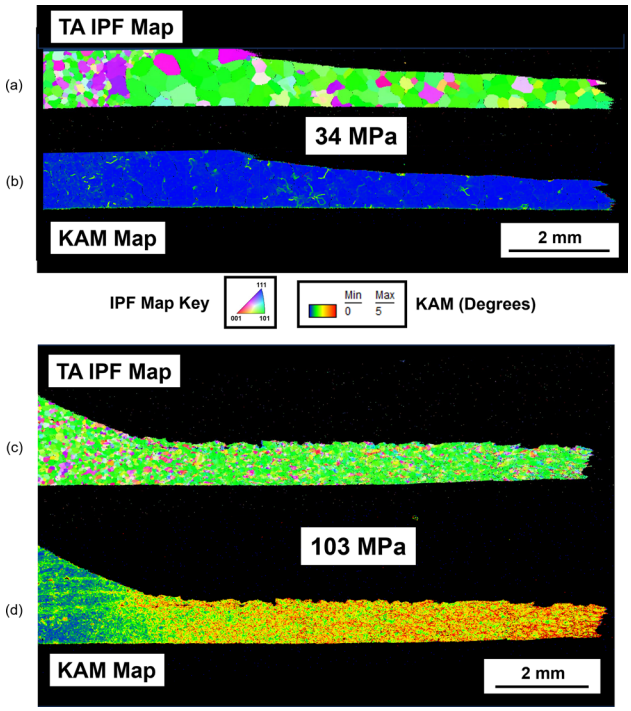


Fig. 7—EBSD data from the midplane of annealed niobium CSCHR sheet samples tested using a heating rate of 63 °C/min and a stress of (*a*), (*b*) 34 MPa or (*c*), (*d*) 103 MPa. The data comprise (a), (c) tension-axis IPF maps and (b), (d) KAM maps (Color figure online).

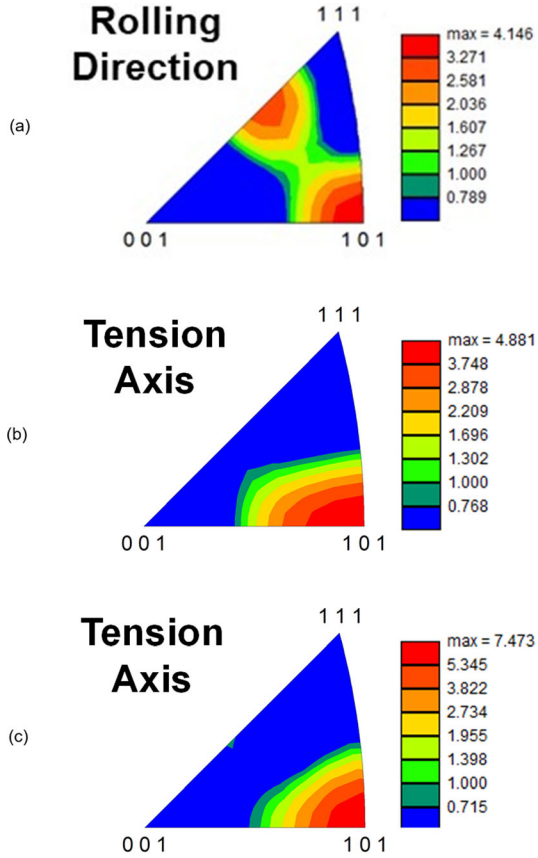


Fig. 8—Rolling-direction/tension-axis inverse pole figures for niobium samples (*a*) in the starting (annealed) condition and (*b*), (*c*) after CSCHR testing to failure at a stress of 103 MPa and heating rate of 63 °C/min. The results for the deformed sample were averaged over (b) the entire reduced section or (c) a 2.5-mm length of the reduced section adjacent to the fracture end (Color figure online).

Table II. Taylor Factors (Heating Rate = 63 °C/min)

| Stress | Location | $M$ ($r$ = 3) | $M$ ($r$ = 1) |
|---|---|---|---|
| 69 | gage section | 3.123 | 3.013 |
| 69 | shoulder | 3.002 | 2.931 |
| 103 | gage section | 3.145 | 2.96 |
| 103 | shoulder | 3.081 | 2.926 |

Slip assumed to occur along <111> directions on {110}, (112), and {123} planes.

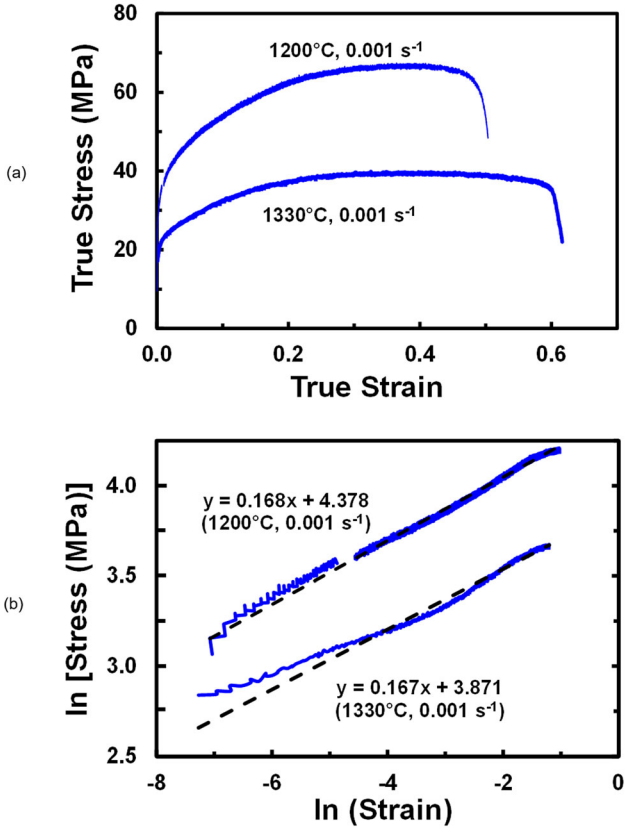


Fig. 9—True stress–true strain data for isothermal tension tests for annealed niobium samples tested along the original RD of the sheet: (*a*) Flow curves and (*b*) corresponding ln stress–ln strain data.

$\dot{\varepsilon}\exp(Q/RT)$), introduced in the pioneering work of Zener and Hollomon in the 1940s dealing with *ambient-temperature* deformation of steels.[23,24] The formulations were generally of the following form[25–31]:

$$\dot{\varepsilon} = A\left(\frac{\sigma}{E}\right)^{n} \exp\left(-\frac{Q}{RT}\right), \qquad [1]$$

where $\dot{\varepsilon}$ denotes the strain rate, $A$ is a constant, $\sigma$ is the applied stress, $E$ is Young's modulus, $n$ is the stress exponent of the strain rate, $Q$ is the apparent activation energy, $R$ is the gas constant, and $T$ is absolute temperature. Later efforts expanded upon such formulations in an attempt to correlate measured (apparent) activation energies to diffusional mechanisms and take microstructural variables (such as grain size) into account.[25,32]

In a formal sense, $Z$-based correlations of flow stress apply to a fixed state of strain/stored work. Because CSCHR tests *at warm-working temperatures* involve continuous changes in strain/work *and* strain rate, a constitutive model which explicitly incorporates strain must be utilized. In the present work, the following simple expression was used for this purpose:

$$\sigma = C\varepsilon^{p}\dot{\varepsilon}^{m} \exp\left(\frac{mQ}{RT}\right), \qquad [2]$$

in which $C$ is a constant, $p$ is the strain-hardening exponent, $m$ is the strain-rate sensitivity (equal to the inverse of the stress exponent $n$). Both $p$ and $m$ are also assumed to be constant. For the case in which $p = 0$ (no strain hardening) and the temperature dependence of $E$ is negligible (*thus, enabling E to be incorporated with the constant in either relation*), it is easy to show that Eqs. [1] and [2] are equivalent. With regard to the assumed constancy of $E$, Brady and Taleff[17] have shown that the polycrystalline (unrelaxed) dynamic elastic Young's modulus of randomly textured Nb is approximately constant at 104.9 GPa from room temperature up to 1300 K and decreases little (to a value of ~ 102 GPa) for temperatures from 1300 K to 1800 K.

It is also important to note that both Eqs. [1] and [2] assume that texture hardening/softening is negligible, as was found for annealed unalloyed niobium in the present investigation, although a general expression incorporating such effects is readily derived.[12] Moreover, it should be emphasized that $\varepsilon$ is used only as an avatar for the stored work even though it is not a state variable. Alternate state variables (*e.g.*, dislocation density) might be more appropriate to describe strain hardening, but would complicate the analysis. Despite this approximation, however, a number of useful results can be obtained and are described next with a specific reference to the interpretation of the present CSCHR data.

A relation for the apparent activation energy $Q$ (pertinent to both CSCHR and isothermal types of tests) is derived first by taking the natural logarithm of both sides of Eq. [2] and differentiating with respect to inverse temperature ($1/T$). Noting that $C$ is a constant, this leads to the following expression:

$$\frac{\partial \ln \sigma}{\partial(1/T)} = p\frac{\partial \ln \varepsilon}{\partial(1/T)} + m\left(\frac{\partial \ln \dot{\varepsilon}}{\partial(1/T)}\right) + \left(\frac{mQ}{R}\right), \qquad [3]$$

which for the case of constant stress becomes after re-arrangement

$$\frac{Q}{R} = -\left(\frac{p}{m}\right)\frac{\partial \ln \varepsilon}{\partial(1/T)} - \left(\frac{\partial \ln \dot{\varepsilon}}{\partial(1/T)}\right). \qquad [4]$$

Equation [4] indicates that $Q/R$ is dependent on two terms, one related to the slope of the Arrhenius plot (second term on the right-hand side (RHS) of the equation) and the other to the rate of change of strain with respect to inverse temperature *and* the ratio of $p$ to $m$ (first term on the RHS). For a non-strain-hardening material, $p = 0$ and the normalized activation energy, $Q/R$, is simply equal to the negative of the slope of the Arrhenius plot. If the state of strain hardening is changing continuously (as it is during CSCHR tests) or is different when comparing strain rate/temperature combinations that yield the same stress for isothermal tests, this term *must* be included in estimating $Q/R$. From a physical perspective, strain hardening tends to *reduce* the strain rate which is generated (at a constant stress) as the temperature is increased during CSCHR testing and thus makes the Arrhenius slope *shallower* than that corresponding to the true

value of $Q/R$. Conversely, a material which exhibits flow softening (due to microstructural sources, for example) will tend to have an Arrhenius slope which is *steeper* than that exhibited in the absence of flow softening.

Several other useful results specific for CSCHR data can be derived by examining a variational form of Eq. [2]. After taking the natural logarithm of both sides and remembering that $C$ is a constant, *viz.*, this relation is the following equation:

$$\delta \ln \sigma = p\delta \ln \varepsilon + m\,\delta \ln\left(\frac{\partial \varepsilon}{\partial T}\alpha\right) + \delta\left(\frac{mQ}{RT}\right). \qquad [5]$$

Here, the term related to the strain rate has been expressed as $\left(\frac{\partial \varepsilon}{\partial T}\right)\cdot\alpha$, in which $\alpha$ denotes the imposed *constant* heating rate ($\mathrm{d}T/\mathrm{d}t$). At fixed strain *and* heating rate [Figure 10(a)], Eq. [5] becomes

$$\delta \ln \sigma = +m\,\delta \ln\left(\frac{\partial \varepsilon}{\partial T}\right) + \left(\frac{mQ}{R}\right)\delta(1/T), \qquad [6]$$

or, after re-arrangement,

$$m = \frac{\delta \ln \sigma}{\delta \ln\left(\frac{\partial \varepsilon}{\partial T}\right) + \frac{Q}{R}\delta(1/T)}. \qquad [7]$$

At fixed temperature *and* heating rate [Figure 10(b)], Eq. [5] becomes after re-arrangement:

$$p = \frac{\delta \ln \sigma - m\delta \ln(\partial \varepsilon/\partial T)}{\delta \ln \varepsilon}. \qquad [8]$$

Last, a useful expression for estimating the ratio of $p$ to $m$ is obtained from Eq. [5] for the case involving fixed stress *and* temperature [Figure 10(c)], *i.e.*,

$$\frac{p}{m} = \frac{-\delta \ln \alpha - \delta \ln\left(\frac{\partial \varepsilon}{\partial T}\right)}{\delta \ln \varepsilon}. \qquad [9]$$

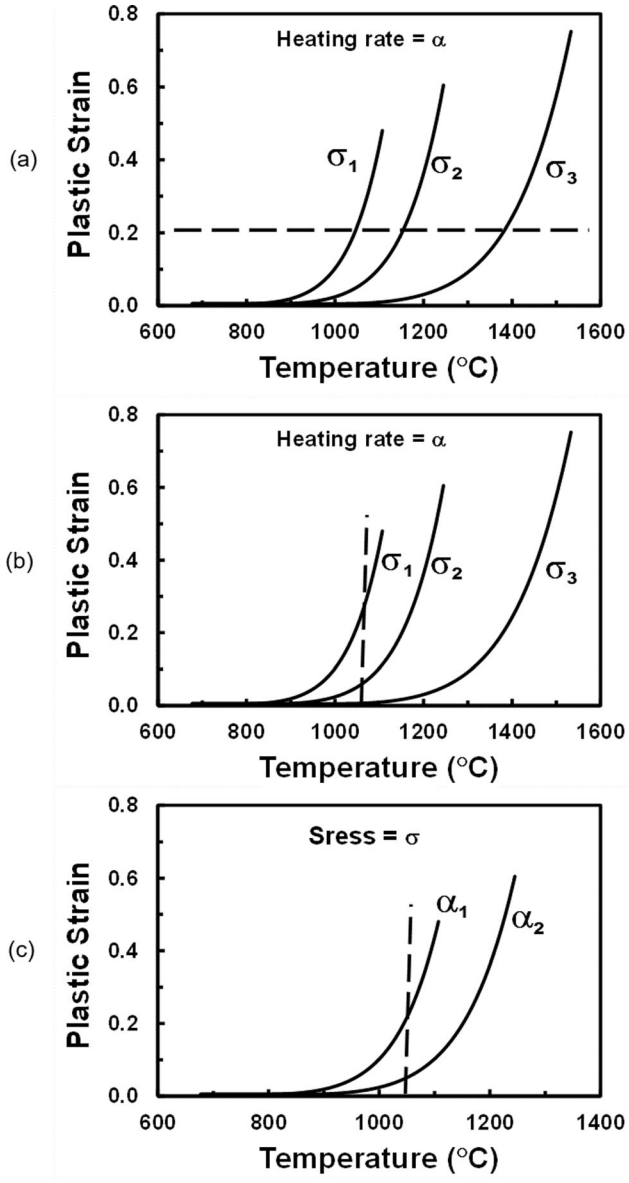


Fig. 10—Schematic illustrations of the constructs used to estimate material coefficients ($m$, $p$) from CSCHR data: (*a*) constant strain and heating rate (for $m$), (*b*) fixed temperature and heating rate (for $p$), and (*c*) fixed stress and temperature (for $p/m$).

## B. *Material Coefficients for Niobium*

The relations developed in the previous section were applied to the CSCHR measurements for annealed unalloyed niobium to determine the various material coefficients in the constitutive relation given by Eq. [2].

Using Eq. [4], the value of $Q/R$ was determined from the sum of (i) the average slope of the Arrhenius plots ($= -22 \times 10^3$ K) (Table I) and (ii) the product of $p/m$ and best-fit slopes of $\ln \varepsilon$ *vs* $1/T$ plots of the CSCHR data. Per Eq. [9], the average value of $p/m$ was derived from measurements of $\varepsilon$ and $\partial\varepsilon/\partial T$ for CSCHR data at various fixed temperatures and stresses for the two heating rates in the present work [Figure 10(c)]. The $p/m$ results showed some scatter (Table III), largely associated with the determination of $\partial\varepsilon/\partial T$. Neglecting the datum for $T = 1400$ °C ($p/m = 0.3$) because it likely lay in the hot-deformation regime ($T/T_{MP} = 0.6$, in which $T_{MP}$ denotes the melting point of niobium), the average value of $p/m$ was estimated to be $1.60 \pm 0.31$. Plots of $\ln\varepsilon$ *vs* $1/T$ (for strains $\geq 0.005$) were nearly linear, but the slope showed some variation with stress level and, hence, temperature experienced during each test (Figure 11; Table IV). The general trend comprised

**Table III. Values of $p/m$ Derived from CSCHR Tests at 15 and 63 °C/min**

| Stress (MPa) | Temperature (°C) | $p/m$ |
|---|---|---|
| 103 | 950 | 1.62 |
| 103 | 1000 | 1.32 |
| 34 | 1300 | 2.03 |
| 34 | 1350 | 1.45 |
| 34 | 1400 | 0.30 |

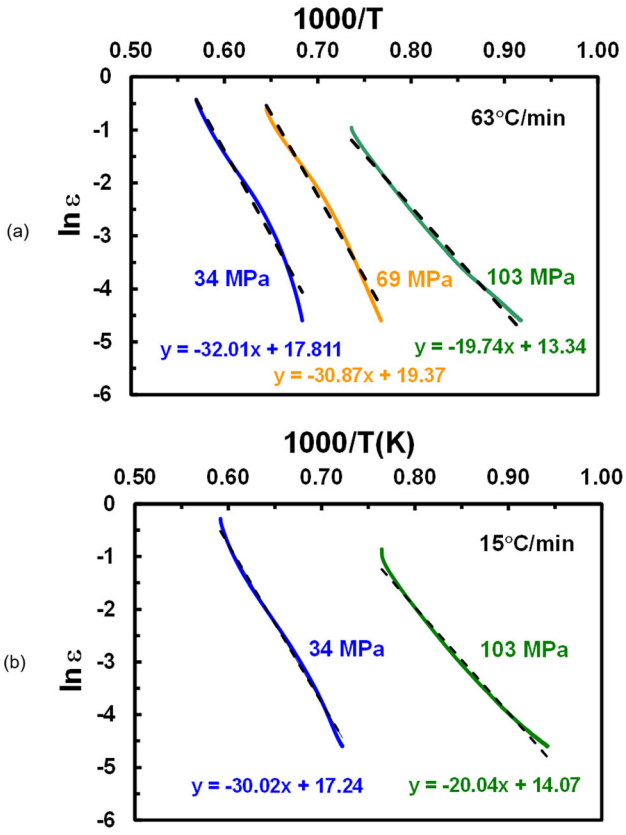


Fig. 11—Plots of lnε as a function of $1/T$ for CSCHR data from tests on annealed niobium sheet samples performed using a heating rate of either (*a*) 63 °C/min or (*b*) 15 °C/min.

an increasing slope with increasing temperature. Nevertheless, an average value ($= -25.4 \pm 5.5 \times 10^3$ K) was obtained by weighting the $\sigma = 34$ MPa data by one-half compared to those for lower temperatures/higher stress levels because the former included data for $T/T_{MP} \geq 0.6$. The overall value of $Q/R$ was thus $22 \times 10^3 + 1.6 \times 25.4 \times 10^3 = 62.6 \times 10^3$ K, resulting in $Q = 521$ kJ/mol.

An average value of the strain-rate sensitivity, $m$, was obtained by applying Eq. [7] to data at a series of fixed strain levels for each heating rate [Figure 10(a)]. A summary of such calculations (Table V) showed little dependence on strain level but some variation depending on the specific stress levels used in Eq. [7]. When using stress levels of 34 and 103 MPa to establish $\delta \ln \sigma$, the value of $m$ was $0.126 \pm 0.003$ (for a heating rate of 63 °C/min) or $0.121 \pm 0.002$ (for a heating rate of 15 °C/min). By contrast, $m$ was $0.089 \pm 0.003$ when using stress levels of 69 and 103 MPa. Because deformation occurred at somewhat lower temperatures for the higher stresses, these results also suggested a weak temperature dependence of $m$ with its value increasing slightly with increasing temperature. For simplicity, an overall average of $m = 0.106$ was used in subsequent calculations to determine the applicability of the constitutive formulation described by Eq. [2].

The value of $p$ was determined from the product of the above estimates of $m$ and $p/m$, *i.e.*, $0.106 \times 1.6 = 0.17$. A similar average (0.16) was obtained from the application of Eq. [8] to the CSCHR data generated at a heating rate of 63 °C/min.

### C. *Evaluation of the Model Fit and Consistency Check*

The applicability of Eq. [2] with the constitutive parameters determined in the previous section ($Q/R = 62.6 \times 10^3$ K (or $Q = 521$ kJ/mol), $m = 0.11$, $p = 0.17$) required an approach involving separation of the variables $\varepsilon$ and $T$ (after replacing $\dot{\varepsilon}$ by the product $(d\varepsilon/dT)\cdot\alpha$) followed by integration. The resulting integral for $T$ led to an infinite series. Hence, Eq. [2] was reduced to a form that could be integrated numerically to yield $\varepsilon(T)$, *i.e.*,

$$\frac{d\varepsilon}{dT} = \alpha^{-1}(\sigma/C)^{1/m}\varepsilon^{-p/m}\exp\left(-\frac{Q}{RT}\right). \qquad [10]$$

in which the constant $C = (1.38\,\text{Mpa}\cdot\text{s}^{0.11})$ was fitted using one measurement for the CSCHR experiment performed for a stress of 103 MPa and heating rate of 63 °C/min.

A comparison of measured strain-*vs*-temperature data (from the CSCHR experiments) and predictions based on the numerical integration of Eq. [2] and the deduced constitutive parameters showed very good agreement (Figure 12), except for the experiment comprising a heating rate of 63 °C/min and stress of 69 MPa. For this case, the predicted strain-*vs*-temperature curve lay somewhat to the left of the measurement [Figure 12(a)]. To investigate the source of this difference, a sensitivity analysis was done using hypothetical variations in the constitutive parameters (Figure 13). As a first example, the effect of a small uncertainty in $Q/R$ on the simulation result was determined. In particular, a variation of 2,000 K (*i.e.*, an increase from 62,600 K to 64,600 K), or a value within the range that was found in Section IV–B, was found to bring the modeled curve into coincidence with the measurement [Figure 13(a)]. Using this improved value of $Q/R$, a relatively small change in the $m$ value (from 0.11 to 0.10) was noted to produce a major deviation of the prediction from the measurement [Figure 13(b)]. Such a sensitivity may be ascribed to the fact that the numerical integration depends on the flow stress raised to the $1/m$ power (Eq. [10]). Last, the sensitivity analysis revealed that a change in the strain-hardening exponent (*e.g.*, from 0.17 to 0.14) has a much smaller, albeit finite, influence on behavior [Figure 13(c)].

The consistency of the constitutive formulation and associated material coefficients was ascertained by analysis of the isothermal tension-test measurements. First, it was noted that the strain-hardening exponent $p$ from the isothermal tests [Figure 9(b)] was essentially identical to that derived from CSCHR data, *i.e.*, 0.17. Furthermore, the overall shape of the flow curve (prior to flow localization) and the magnitude of the flow stresses were well predicted to a reasonable first order

Table IV. Slopes ($10^3$ K) of ln$\varepsilon$ *vs* $1/T$(K) Plots

| Heating Rate (°C/min) | $\sigma$ = 34 MPa | $\sigma$ = 69 MPa | $\sigma$ = 103 MPa |
|---|---|---|---|
| 63 | − 32.0 | − 30.9 | − 19.7 |
| 15 | − 30.0 | — | − 20.0 |

Table V. CSCHR *m* Values

| Heating Rate (°C/min) | Stress Values (MPa) | Strain | *m* |
|---|---|---|---|
| 63 | 34, 103 | 0.05 | 0.122 |
| 63 | 34, 103 | 0.10 | 0.127 |
| 63 | 34, 103 | 0.20 | 0.127 |
| 63 | 34, 103 | 0.30 | 0.128 |
| 63 | 69, 103 | 0.05 | 0.085 |
| 63 | 69, 103 | 0.10 | 0.092 |
| 63 | 69, 103 | 0.20 | 0.091 |
| 63 | 69, 103 | 0.30 | 0.088 |
| 15 | 34, 103 | 0.05 | 0.119 |
| 15 | 34, 103 | 0.10 | 0.121 |
| 15 | 34, 103 | 0.20 | 0.123 |
| 15 | 34, 103 | 0.30 | 0.123 |

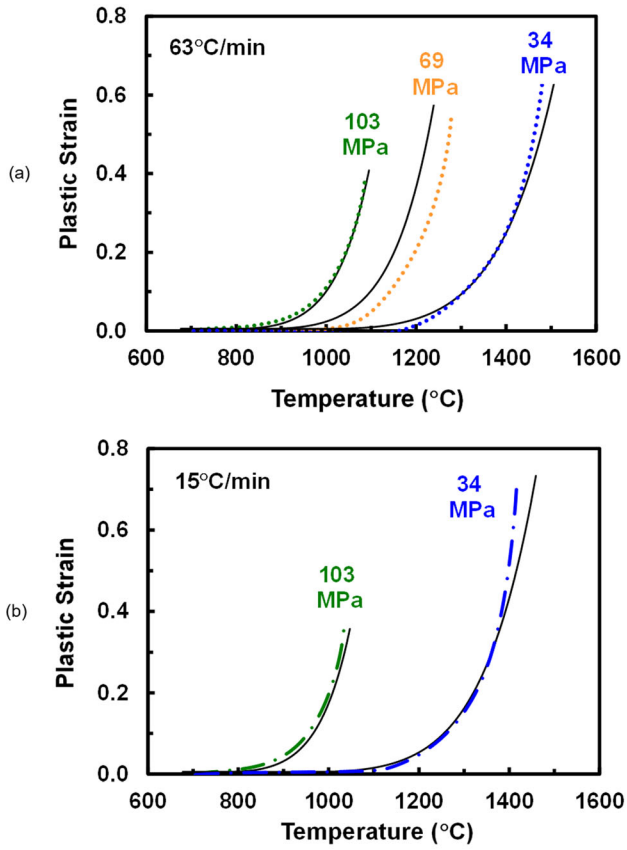


Fig. 12—Comparison of measured strain-*vs*-temperature data (dotted curves) and model predictions (solid black lines) for CSCHR tests on annealed niobium sheet samples performed using applied stresses of 34, 69, or 103 MPa and a heating rate of either (*a*) 63 °C/min or (*b*) 15 °C/min (Color figure online).

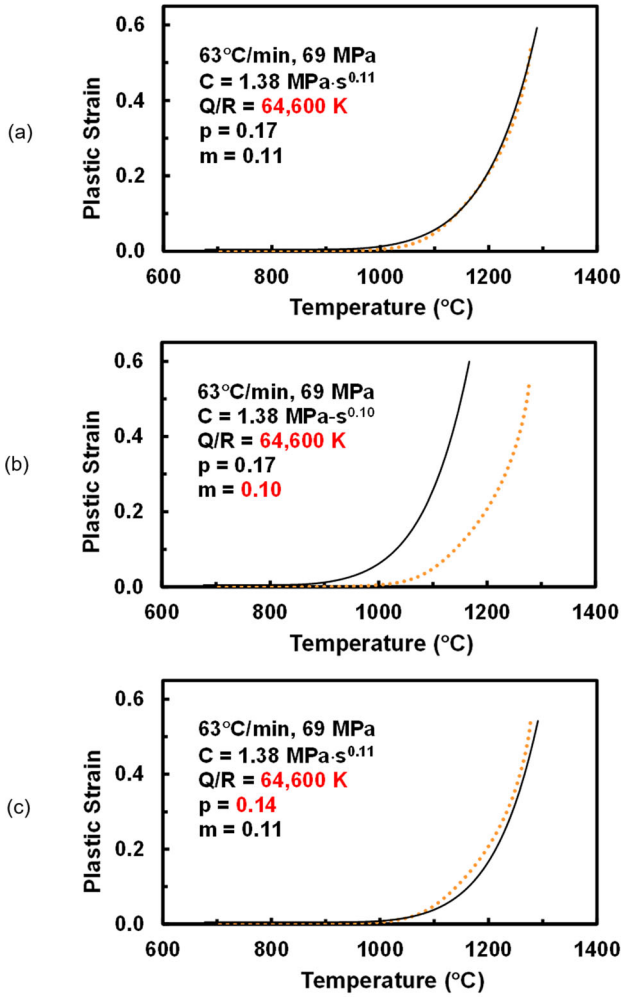


Fig. 13—Sensitivity analysis for CSCHR tests performed using a stress of 69 MPa and a heating rate of 63 °C/min in order to assess the effect on model predictions of the constitutive coefficient (*a*) $Q/R$, (*b*) $m$, or (*c*) $p$. The dotted orange curve in each figure connotes the experimental measurement (Color figure online).

using $C = 1.38\ \text{Mpa}\cdot\text{s}^{0.11}$, $p = 0.17$, $m = 0.11$, and $Q/R$ between 62,600 and 64,600 K (Figure 14).

Finally, predictions from flow-localization simulations based on the load-equilibrium approach showed excellent agreement with the measurements. Specifically, simulations showed the typical dependence of the necking strain (at which the load drop is noticeable) on the values of $m$ and the so-called imperfection factor $f_o$ (Figure 15). The latter parameter quantifies a variation in cross-sectional area or the strength coefficient along the length of the reduced section. A variation in temperature along the reduced section can also be

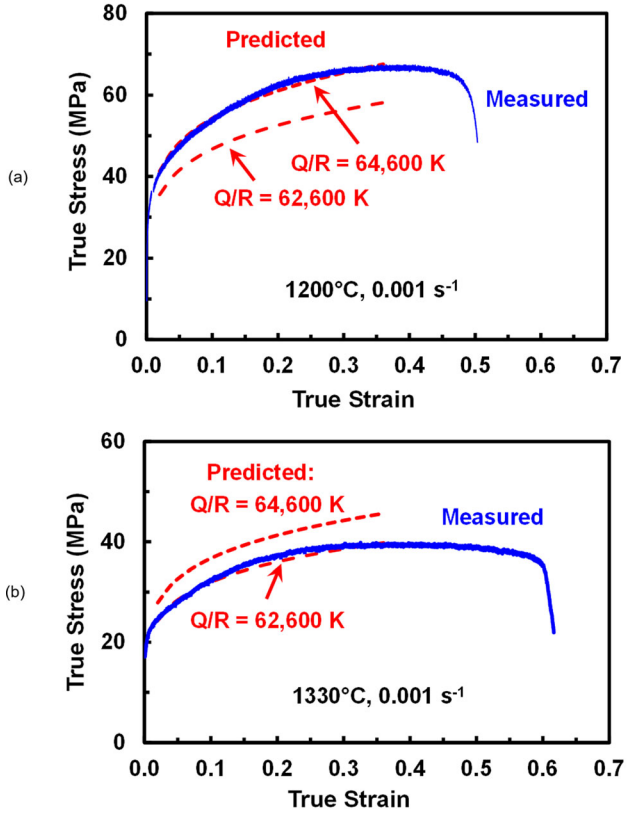


Fig. 14—Comparison of measured isothermal tension-test data for annealed niobium sheet samples tested at a constant strain rate of 0.001 $s^{-1}$ (blue curves) and model predictions using $Q/R$ = 62,600 K or 64,600 K (broken red lines) for a test temperature of (*a*) 1200 °C or (*b*) 1330 °C (Color figure online).

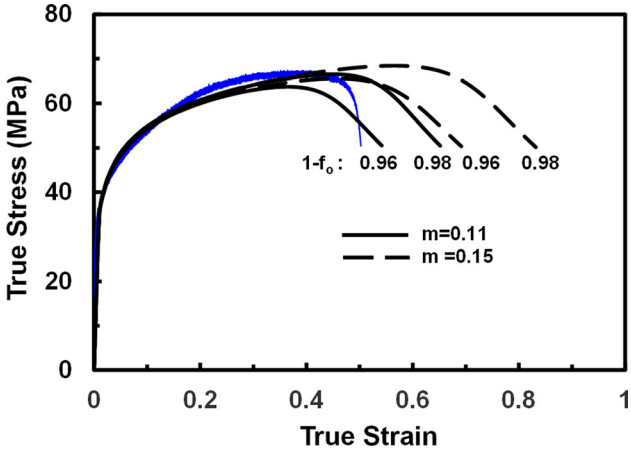


Fig. 15—Comparison of the isothermal tension-test flow curve measured for 1200 °C/0.001 $s^{-1}$ (blue curve) and predictions from flow-localization calculations using two different values of the rate sensitivity $m$ and two different values of the imperfection factor $f_o$ (solid and broken black lines) (Color figure online).

associated with $f_o$. For example, a 2-degree variation in axial temperature would give rise to an $f_o$ of 0.95 for $Q/R$ = 62,600 K. A comparison of the measured stress–strain curve for 1200 °C/0.001 $s^{-1}$ with flow-localization simulations showed the best fit using $m$ = 0.11 and $f_o$ between 0.96 and 0.98 (Figure 15). This value of $m$ coincided with that deduced from CSCHR testing of niobium. Moreover, experience has shown that $f_o \sim 0.98$ often provides the best fit to observed necking strains.[33]

The present constitutive parameters also compared favorably to values derived from the isothermal, constant-strain-rate tension data reported by Brady and Taleff.[17] This comparison is summarized in Appendix A.

## V. FUTURE WORK

To the best of the authors' knowledge, the present work represents the first attempt to quantify the simultaneous and discrete effects of strain- and strain-rate hardening on the apparent activation energy of a metallic material. The approach utilized a rather simple engineering stress–strain relation which was capable of providing consistent results for both constant-stress, constant-heating-rate (CSCHR), and isothermal-tension tests. The present results and interpretation suggest several possible endeavors for future research. These include the following:

- It would be useful to investigate constitutive formulations that incorporate internal state variables (*e.g.*, dislocation density) rather than strain *per se* to describe the state of strain hardening.
- Isothermal, strain-rate jump tests would be useful to establish $m$ as a function of strain, strain rate, and temperature and provide data that could be compared to $m$ values derived from continuous (isothermal) flow curves as well as CSCHR tests.
- Although the present work focused primarily on the warm-deformation regime, similar research that extends to higher (hot-working) temperatures (at which strain-hardening might be limited) would be useful to establish the apparent activation energy and, thus, help determine the micro-mechanisms that control this quantity over a wider range of temperatures.

## VI. SUMMARY AND CONCLUSIONS

A suite of constant-stress, constant-heating-rate (CSCHR), and isothermal-tension tests was performed to establish a consistent set of material coefficients that could describe the deformation behavior of annealed (Type 1) niobium in the warm-deformation regime. The following conclusions were drawn from this work:

1. Assuming a relatively simple constitutive formulation, the flow-stress dependence on strain, strain rate, and temperature can be described for both CSCHR and isothermal modes of deformation using the same set of material coefficients.
2. The activation energy $Q$ for a strain-hardening material depends on two terms. For data from CSCHR tests, the first term comprises the slope of a standard Arrhenius plot. The second term

quantifies the effect of strain hardening on behavior and comprises the product of (i) the ratio of the strain hardening ($p$) and strain-rate sensitivity ($m$) exponents and (ii) the slope of a plot of $\ln\varepsilon$ as a function of inverse absolute temperature. The latter slope appears to depend on stress/temperature. However, an average value of this quantity still provides a reasonably good fit to experimental data for both CSCHR and isothermal-tension results.

3. Relations can be readily derived to extract average values of $p$ and $m$ over the temperature range of interest from CSCHR data obtained at various stress levels and heating rates.
4. With judicious choice of test conditions, a rather small number of CSCHR experiments (*i.e.*, 3 to 5) is required to determine the constitutive parameters for a material which exhibits strain and strain-rate hardening.
5. Future work should be performed to establish (i) the robustness of the measurement technique developed herein for behaviors that extend into the hot-deformation regime and (ii) alternate descriptions of strain hardening such as internal-state-variable approaches.


## ACKNOWLEDGMENTS

This work was conducted as part of the in-house research of the Air Force Research Laboratory's Materials and Manufacturing Directorate. Technical discussions with Dr. A.A. Salem are gratefully acknowledged. Three of the authors (SLS, NCL, and PNF) were supported under the auspices of Air Force Contract FA8650-21-D-5270. Two of the authors (TJB and EMT) were supported under the auspices of National Science Foundation Grant DMR-2003312.


## CONFLICT OF INTEREST

On behalf of all authors, the corresponding author states that there is no conflict of interest.

## APPENDIX A

The analysis in the present work and the material coefficients so determined have spurred a re-examination of prior isothermal, tension-test work (using the same lot of Type 1 niobium material), which was performed by Brady and Taleff.[17] Despite the use of material from the same lot, however, sample preheat times in the prior work were substantially longer and thus gave rise to larger grain sizes (~ 75 to 280 $\mu$m) compared to the annealed condition in the present work for which the grain size was ~ 40 $\mu$m. Keeping in mind this difference in grain size, attention was focused herein on a comparison of values of the strain-hardening exponent ($p$), the strain-rate sensitivity ($m$), and the normalized apparent activation energy ($Q/R$) deduced from analysis of the prior isothermal data obtained for strain rates of $10^{-4}$ and $10^{-3}$ $s^{-1}$ and temperatures of 1200 °C and 1300 °C.

First, ln–ln plots of the Brady-and-Taleff (B&T) flow curves at $10^{-3}$ $s^{-1}$ revealed substantial flow hardening with a slope of ~ 0.26 or 0.30 [Figure 16(a)]. These slopes were noticeably greater than that found here, *i.e.*, 0.17. The presence of a soft initial texture (associated with grain growth) coupled with texture *hardening* (associated with crystal rotations toward the <101> direction) were, thus, examined as a possible explanation of the difference. To investigate this possibility, the *isothermal* constitutive relation was written as the following:

$$\sigma = C^* M \varepsilon^p, \qquad [11]$$

in which $C^*$ is a constant, $M$ denotes the instantaneous Taylor factor as a function of strain, and $p$ is the strain-hardening exponent as before.

Taking the natural log of both sides of Eq. [11] and differentiating with respect to $\varepsilon$ yields an expression for the overall flow hardening rate:

$$\mathrm{d}\ln\sigma/\mathrm{d}\ln\varepsilon = (\mathrm{d}\ln M/\mathrm{d}\ln\varepsilon) + p. \qquad [12]$$

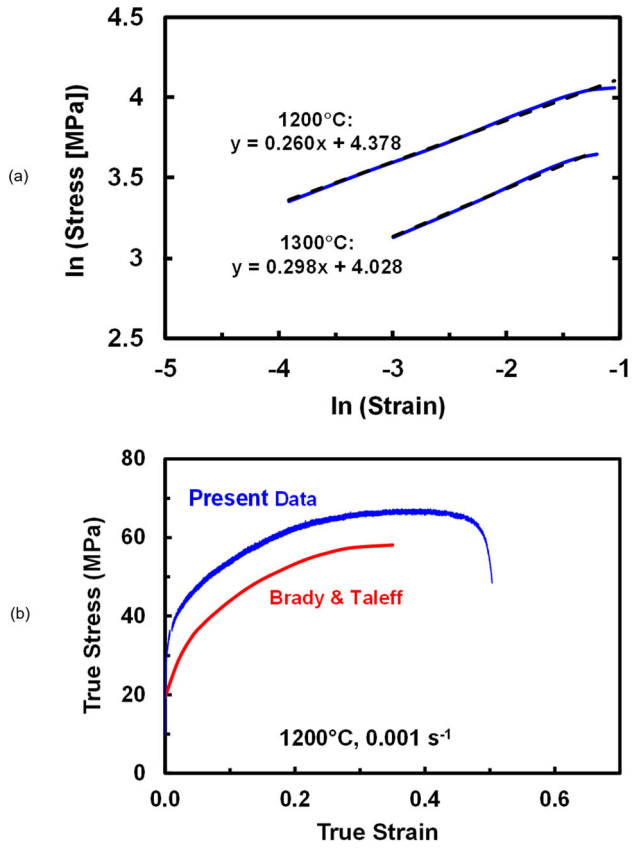


Fig. 16—Analysis of isothermal flow stress results from Ref. 17: (*a*) Ln–ln plots of stress–strain data determined at a strain rate of 0.001 $s^{-1}$ and temperatures of 1200 °C and 1300 °C and (*b*) comparison of flow curves determined at 1200 °C and 0.001 $s^{-1}$ from the present and prior work.

Thus, the flow hardening rate is the sum of the texture-hardening/softening rate ($d\ln M/d\ln\varepsilon$) and the strain-hardening exponent $p$. Because texture measurements after deformation were not available in Reference 17, the texture-hardening rate was estimated by comparing the B&T flow curve at 1200 °C, $10^{-3}$ $s^{-1}$ to the isothermal one measured under the same conditions in the present work [Figure 9(a)] for which texture hardening was (serendipitously) found to be very low. This comparison of isothermal flow curves did indeed reveal substantially lower stresses for the B&T measurement [Figure 16(b)]. Neglecting the very small change in texture in the present flow curve, the *increase* in the flow-stress ratio ($\sigma_{B\&T}/\sigma_{present}$) from $\varepsilon = 0.02$ to $\varepsilon = 0.30$ was used to estimate the average flow hardening rate due to texture change in the B&T experiments. This increase corresponded to 0.70 (at $\varepsilon = 0.02$) to 0.885 (at $\varepsilon = 0.3$) of the assumed constant $M$ for the present data, thus, yielding an average texture-hardening rate of $[\ln(0.885/0.70)]/[\ln(0.30/0.02)] = 0.087$. Adding this quantity to $p = 0.17$ gave an estimated overall flow hardening rate of ~ 0.26, a value identical to the measurement for 1200 °C/0.001 $s^{-1}$ [Figure 16(a)]. The slightly higher value of the overall flow hardening rate at 1300 °C (0.30) [Figure 16(a)] may be hypothesized to have resulted from the evolution of a slightly softer starting texture in the B&T material due to additional grain growth during the 1-hour preheat at the higher temperature.

It was also of interest to determine and examine values of strain-rate sensitivity that can be derived directly from the B&T isothermal data for a temperature of 1200 °C and strain rates of $10^{-4}$ $s^{-1}$ and $10^{-3}$ $s^{-1}$. Two different methods were employed for this purpose. The first, or more conventional, approach compared the stresses at identical levels of strain for the flow curves determined at the two different strain rates. The results (Table VI) gave values of $m$ that showed a weak dependence of $m$ on strain. The average value of $m$ over the entire range of strain was 0.145. The second method involved comparing the stresses for the two different strain rates at *equivalent levels of plastic work per unit volume* in an attempt to mimic the conditions that would pertain in a strain-rate-jump test. Such an approach assumed of course that the Taylor-Quinney factor[34] for the fraction of work that is converted to heat (and hence the fraction retained in the form of defects such as dislocations) was identical for the two strain rates. Flow curves replotted in terms of stress *vs* instantaneous work per unit volume are summarized in Figure 17, and the resulting $m$ values are listed in Table VII. As for the results from the first method, $m$ showed a weak dependence on the independent variable (work per unit volume) (Table VII). Nevertheless, the average value of $m$ was ~ 0.11, a number equal to that determined from the present CSCHR experiments.

Brady and Taleff[17] also estimated a value of the normalized apparent activation energy (*i.e.*, $Q/R$ ~ 54,600 K) from their isothermal flow-stress data at large strains (0.35) at which the stored work was likely somewhat comparable in the various samples. The contribution to $Q/R$ of a term involving strain (analogous to the first term on the RHS of Eq. [4] for CSCHR data) could, therefore, be rightfully neglected and $Q/R$ determined solely based on the corresponding Arrhenius slope. The degree of approximation in using this approach was assessed by comparison to the value of $Q/R$ determined from the present CSCHR measurements, *i.e.*, 62,600 K, although the apparent scatter in these current measurements ($\pm$ (1.6 × 5000) = $\pm$ 8000 K) was indeed comparable to the scatter in the former data of Brady and Taleff.[17]

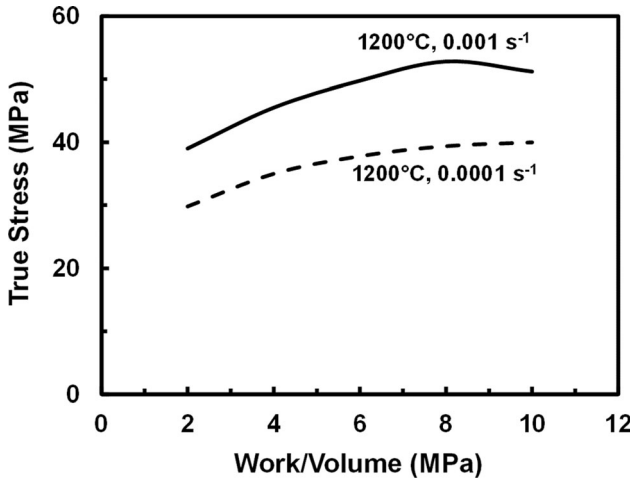


Fig. 17—Replot of isothermal flow stress data for 1200 °C from Ref. 17 in terms of stress as a function of work per unit volume.

**Table VI. B&T *m* Values at 1200 °C ($\sigma$'s at Equivalent Strains)**

| Strain | *m* |
|---|---|
| 0.05 | 0.142 |
| 0.10 | 0.139 |
| 0.15 | 0.145 |
| 0.20 | 0.149 |
| Average | 0.144 |

**Table VII. B&T *m* Values at 1200 °C ($\sigma$'s at Equivalent Work/Volume)**

| Wk/Vol (MPa) | *m* |
|---|---|
| 2 | 0.117 |
| 4 | 0.114 |
| 6 | 0.119 |
| 8 | 0.127 |
| 10 | 0.107 |
| Average | 0.117 |

## REFERENCES


1. *High-Temperature Refractory Metals, Volume 34, Metallurgical Society Conferences*, R.W. Fountain, J. Maltz, and L.S. Richardson, eds., Gordon and Breach Science Publishers, Inc., New York, 1966.
2. *Refractory Alloy Technology for Space and Nuclear Power Applications*, Report CONF-8308-130, R.H. Cooper and E.E. Hoffman, eds., Office of Scientific and Technical Information, US Department of Energy, Washington, DC, 1984.
3. *Refractory Metals*, *Chapter 31, Elements of Metallurgy and Engineering Alloys*, F.C. Campbell, ed., ASM International, Materials Park, OH, 2008, pp. 583–96.
4. N.R. Philips, M. Carl, and N.J. Cunningham: *Metall. Mater. Trans. A*, 2020, vol. 51A, pp. 3299–310.
5. C.C. Wojcik and W. Chang: in *Proc. Inter. Symp. on Niobium 2001*, Orlando, FL, 2001, pp. 163–73.
6. *High-temperature Oxidation-Resistant Coatings*, G.M. Pound, ed., National Academy of Sciences/National Academy of Engineering, Washington, DC, 1970.
7. R.A. Perkins and G.H. Meier: *JOM*, 1990, vol. 42(8), pp. 17–21.
8. O.N. Senkov, D.B. Miracle, and S.I. Rao: *Mater. Sci. Eng. A*, 2021, vol. A820, paper #141512.
9. C. Ren, Z.Z. Fang, M. Koopman, B. Butler, J. Paramore, and S. Middlemas: *Int. J. Refract. Mater.*, 2018, vol. 75, pp. 170–83.
10. O.N. Senkov, D.B. Miracle, K.J. Chaput, and J.-P. Couzinie: *J. Mater. Res.*, 2018, vol. 33, pp. 3092–128.
11. S.L. Semiatin, P.N. Fagin, N.C. Levkulich, B.T. Gockel, B.F. Antolovich, E.M. Crist, J. Cormier, and J.S. Tiley: *Metall. Mater. Trans. A*, 2022, vol. 53A, pp. 394–406.
12. S.L. Semiatin, N.C. Levkulich, and T.M. Butler: *Metall. Mater. Trans. A*, 2024, vol. 55A, pp. 375–88.
13. *ASTM Standard B393-18*, ASTM International, West Conshohocken, PA, 2018.
14. G. Brinson and B.B. Argent: *J. Inst. Met.*, 1962–1963, vol. 91, pp. 293–98.
15. M.J. Klein and M.E. Gulden: *Metall. Trans.*, 1973, vol. 4, pp. 2175–80.
16. A.N. Behera, R. Kapoor, A. Sarkar, and J.K. Chakravartty: *Mater. Sci. Technol.*, 2014, vol. 30, pp. 637–44.
17. E.A.D. Brady and E.M. Taleff: *Metall. Mater. Trans. A*, 2021, vol. 52A, pp. 1095–105.
18. E.A.D. Brady and E.M. Taleff: *Metall. Mater. Trans. A*, 2022, vol. 53A, pp. 3057–072.
19. S. Butterworth: *Exp. Wirel.*, 1930, vol. 7, pp. 536–41.
20. T. Haslwanter: *Hands-On Signal Analysis with Python: An Introduction*, Springer Inter'l Publishing, Cham, 2021, pp. 71–104.
21. S.L. Semiatin, A.K. Ghosh, and J.J. Jonas: *Metall. Trans. A*, 1985, vol. 16A, pp. 2291–98.
22. J.M. Rosenberg and H.R. Piehler: *Metall. Trans.*, 1971, vol. 2, pp. 257–59.
23. C. Zener and J.H. Hollomon: *J. Appl. Phys.*, 1944, vol. 15, pp. 22–32.
24. C. Zener and J.H. Hollomon: *Trans. ASM*, 1944, vol. 33, pp. 163–235.
25. O.D. Sherby and P.M. Burke: *Prog. Mater. Sci.*, 1968, vol. 13, pp. 325–90.
26. O.D. Sherby: *Acta Metall.*, 1962, vol. 10, pp. 135–47.
27. C.R. Barrett, A.J. Ardell, and O.D. Sherby: *Trans. AIME*, 1964, vol. 230, pp. 200–04.
28. M.Y. Wu and O.D. Sherby: *Acta Metall.*, 1984, vol. 32, pp. 1561–72.
29. O.A. Ruano and O.D. Sherby: *Rev. Phys. Appl.*, 1988, vol. 23, pp. 625–37.
30. O.A. Ruano, J. Wadsworth, and O.D. Sherby: *Acta Metall.*, 1988, vol. 36, pp. 1117–128.
31. M.E. Kassner: *Fundamentals of Creep in Metals and Alloys*, Butterworth-Heinemann, Waltham, MA, 2015, pp. 9–91.
32. J.E. Bird, A.K. Mukherjee, and J.E. Dorn: in *Quantitative Relation Between Microstructure and Properties*, D.G. Brandon and A. Rosen, eds., Israel Universities Press, Jerusalem, Israel, 1969, pp. 255–342.
33. S.L. Semiatin and J.J. Jonas: *Formability and Workability of Metals: Plastic Instability and Flow Localization*, ASM, Metals Park, OH, 1984.
34. G.I. Taylor and H. Quinney: *Proc. R. Soc. Lond.*, 1934, vol. 143, pp. 307–26.